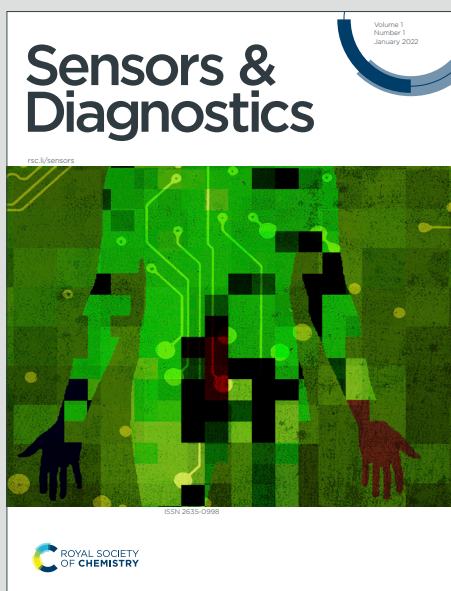


# Sensors & Diagnostics

Accepted Manuscript

This article can be cited before page numbers have been issued, to do this please use: V. Vezza, V. Mani, N. Docherty, A. Butterworth, D. Alcorn, P. A. Hoskisson and D. Corrigan, *Sens. Diagn.*, 2025, DOI: 10.1039/D5SD00210A.



This is an Accepted Manuscript, which has been through the Royal Society of Chemistry peer review process and has been accepted for publication.

Accepted Manuscripts are published online shortly after acceptance, before technical editing, formatting and proof reading. Using this free service, authors can make their results available to the community, in citable form, before we publish the edited article. We will replace this Accepted Manuscript with the edited and formatted Advance Article as soon as it is available.

You can find more information about Accepted Manuscripts in the [Information for Authors](#).

Please note that technical editing may introduce minor changes to the text and/or graphics, which may alter content. The journal's standard [Terms & Conditions](#) and the [Ethical guidelines](#) still apply. In no event shall the Royal Society of Chemistry be held responsible for any errors or omissions in this Accepted Manuscript or any consequences arising from the use of any information it contains.

## Low-Cost printed circuit board (PCB) electrochemical biosensors for rapid and label-free detection of *Streptococcus pneumoniae*

View Article Online  
DOI: 10.1039/D5SD00210A

Vincent Vezza,<sup>1</sup> Veerappan Mani,<sup>1</sup> Niamh Docherty,<sup>1</sup> Adrian Butterworth,<sup>1</sup> David Alcorn<sup>2</sup>,  
Paul A. Hoskisson<sup>3</sup>, Damion Corrigan<sup>1\*</sup>

<sup>1</sup> University of Strathclyde, Centre for Advanced Measurement Science and Health Translation, Pure and Applied Chemistry, Thomas Graham Building, 295 Cathedral St, Glasgow G1 1XL, UK

<sup>2</sup> Department of Anaesthesia, Royal Alexandra Hospital, Corsebar Rd, Paisley, PA2 9PN, UK.

<sup>3</sup> Strathclyde Institute of Pharmacy and Biomedical Sciences, 161 Cathedral St, Glasgow G4 0RE, UK.

\*corresponding author email: damion.corrigan@strath.ac.uk

**Abstract** Severe sepsis presents a critical healthcare challenge where rapid pathogen identification is vital for timely intervention. Current diagnostic methods, however, remain inadequate, often delaying targeted treatment. Using readily available printed circuit board (PCB) electrodes, we address this need by developing a low-cost electrochemical DNA biosensor for rapid detection of *Streptococcus pneumoniae* using the *lytA* gene as biomarker. Through systematic evaluation of commercial and custom PCB designs (P1-P4), gold-plated PCB P4 was found as the optimal platform, demonstrating sensitive detection of *lytA* sequences (20 bp at 4.50 pM limit of detection in buffer) and clinically relevant 235 bp polymerase chain reaction (PCR) amplicons in 100% of human serum (1.0-100 pM) within 15 min at room temperature using electrochemical impedance spectroscopy. The performance of the biosensor originates from optimized electrode geometry, surface properties, and robust self-assembled monolayer functionalization, enabling specific recognition of bacterial DNA without sample pretreatment. This work establishes PCB-based biosensors as a promising solution for point-of-care sepsis diagnostics, offering significant advantages in speed, cost, and operational simplicity compared to conventional methods.



## 1. Introduction

View Article Online  
DOI: 10.1039/D5SD00210A

Severe Sepsis is a life-threatening medical emergency that provides a significant challenge to clinicians and health care systems.<sup>1</sup> *The UK Sepsis trust* database indicates that Sepsis is responsible for 11 million deaths globally each year and, and 48,000 sepsis related deaths each year in the UK.<sup>2</sup> Sepsis is an extremely challenging illness to diagnose as there is often a multitude of signs, symptoms and measurements that can occur that can be attributed to many other serious or benign medical conditions.<sup>3</sup> Among the various pathogens responsible for sepsis, *Streptococcus pneumoniae* infection is commonly fatal particularly in cases of community-acquired respiratory infections, highlighting the urgent need for rapid and specific diagnostic tools.<sup>4-6</sup> There is growing demand for a low-cost, rapid point-of-care (PoC) diagnostic device capable of detecting *Streptococcus pneumoniae*, not only in hospitals but also in community screening, primary care, and home healthcare settings.<sup>7</sup>

Phenotypic identification, genotypic identification, and mass spectrometry are the three key methods used for this purpose; the main issue with such methodology is that they can take hours to days to result.<sup>8-10</sup> Phenotypic identification, the current gold standard, relies on culturing blood samples to observe bacterial growth, followed by biochemical testing which typically requires more than 72 hours. Genotypic identification relies on DNA or RNA analysis through techniques like 16S/23S ribosomal DNA sequencing and amplified ribosomal DNA restriction analysis (ARDRA), but they are limited by time consumption, the need for specialized equipment and expertise, and reduced effectiveness in distinguishing closely related strains. Matrix-Assisted laser desorption/ionization time-of-flight mass spectrometry (MALDI-TOF MS) identifies pathogens by analysing their protein mass spectra through laser desorption and time-of-flight measurement, offering rapid, cost-effective detection but is limited by the need for prior colony cultivation (24-48 hours), dependence on reference spectra, and database availability.<sup>10</sup> Notably, all these methods are lab-centric and not suitable for PoC use. Pneumococcal urinary antigen test is the only currently available PoC device that can provide a time to result upon sample application in 15 min, however it require temperature equilibration of samples and reagents, involve multiple manual steps, and their generalizability can be uncertain.<sup>11,12</sup> These drawbacks highlight the need for the development of better PoC devices.

Electrochemical biosensors are a promising solution, offering potential for miniaturization, low cost, and rapid results.<sup>13, 14</sup> Specifically, printed circuit board (PCB)



electrodes are a compelling platform because they have significant advantages, including high customizability through modern design software, established manufacturing processes for rapid, precise, and low-cost mass production, and a variety of available metal plating finishes.<sup>15</sup> <sup>16</sup> Increased electrode numbers can be manufactured on smaller surfaces resulting in higher sample sizes within smaller time intervals. Due to the maturation of PCB systems and their extensive incorporation in modern electronic devices, they can be easily integrated into electrochemical readers. They can have additional electronics easily incorporated onto or conjoined to the electrode system of the end goal device. PCB biosensors have been reported in the literature with a wide range of research applications undertaken.<sup>17</sup> However, a label-free PCB-based DNA sensor for the direct detection of *S. pneumoniae* in clinically relevant matrices like human serum has not been demonstrated.

The main objective of this work is to develop PCB-based low-cost, rapid diagnostic test strips for rapid detection of *Streptococcus pneumoniae*, to tackle existing limitations in sepsis diagnostics. Four different PCBs (P1-P4) have been demonstrated in this work, each having different electrode configurations, size, geometry, surface material, and manufacturing methods (**Figure 1**). The four PCB electrodes were not selected to enable direct comparison between identical surfaces, but rather to represent distinct and practically relevant PCB manufacturing routes: PCB P1: Fully in-house fabricated prototype, PCB P2: Commercially fabricated board with in-house gold plating, PCB P3: Standard commercial fabrication (bare copper), and PCB P4: Commercially fabricated and optimized for biosensing (gold-plated). The aim of the study was to assess how these different fabrication pathways commonly encountered during biosensor development and scale-up, influence electrode surface characteristics and biosensing performance. By functionalising PCB electrodes with a DNA probe sequence that specifically binds a truncated sequence derived from the *S. pneumoniae* *lytA* gene which encodes the major autolysin *LytA*, a label-free *S. pneumoniae* biosensor platform was developed.<sup>18</sup> Amplification of a 235 pb from the *lytA* gene has been shown to electrochemically distinguish *S. pneumoniae* from similar streptococci.<sup>19</sup> Our investigation shows that using a *lytA* probe and a 20 bp sequence from the *lytA* gene and PCB P4 biosensor platform that this target was detectable at 10 pM in buffer with a calculated limit of detection (LoD) of 4.50 pM. The amplified 235 bp *lytA* using primers form was detectable at 1.0 pM in complex human serum with a 15 min time to result at room temperature.



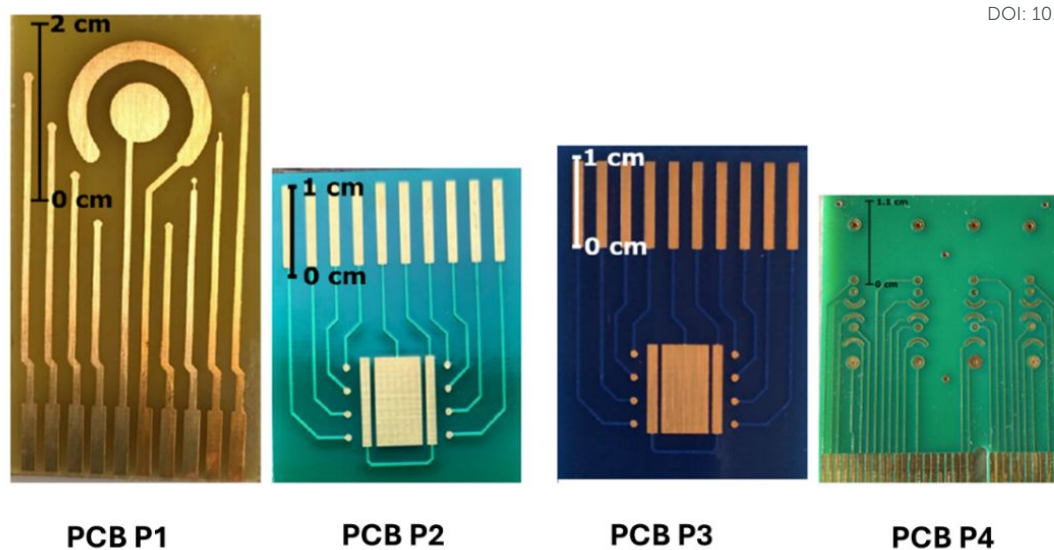


**Figure 1.** PCB designs used in the study. PCB P1: Initial prototype design. PCB P2: Commercially fabricated and hard gold-plated version with an updated layout for improved efficiency and accessory compatibility. PCB P3: Commercially fabricated bare copper board with the same layout as P2 but without gold plating. PCB P4: Purchased from PCB biosensor company, *BIOTIP biodevice technology*.

## 2. Experimental

### 2.1. Reagents

Deionized (DI) water (resistivity  $\geq 18 \text{ M}\Omega\text{cm}$ ), hydrogen peroxide ( $\text{H}_2\text{O}_2$ ), phosphate buffered saline tablets (PBS), potassium chloride (KCl), potassium ferricyanide ( $\text{K}_3[\text{Fe}(\text{CN})_6]$ ), potassium ferrocyanide  $\text{K}_4[\text{Fe}(\text{CN})_6]$ , sulfuric acid ( $\text{H}_2\text{SO}_4$ ), Tris(2-carboxyethyl)phosphine (TCEP), and 3-mercapto-1-propanol (MCP) were purchased from Sigma. Acid piranha solution was prepared by mixing 18.0 M  $\text{H}_2\text{SO}_4$  and 30 %  $\text{H}_2\text{O}_2$  in a volume ratio of 3:1 (v/v). PBS (pH 7.40) is the buffer used throughout the unless otherwise specified. All oligonucleotides (probe, target, and primers) were obtained from Sigma, and their sequences are provided in **Table 1**.

### 2.2. Custom PCB electrodes

Four PCB electrodes featuring 4 different design and geometries, named as PCB P1, PCB P2, PCB P3, and PCB P4. Detailed specifications of all the electrodes are provided in **Table S1**. All PCB boards used the same electrochemical cell setup for the plating process.



Once each board had obtained a gold surface finish it was cleaned to remove any impurities and contaminants. The details about cell configuration for electrode plating and cleaning, plating procedure, and cleaning procedure are given in supporting information (**sections S1-S3, Table S1 & S2, and Figure S1 & S2**). The reference and counter electrode geometries differ between PCB designs as part of an exploratory study into layout efficiency. While these geometric variations can influence absolute electrochemical parameters, all designs were controlled to maintain stable reference potentials and adequate counter electrode competence. The comparative performance assessment focuses on the normalized biosensing response (i.e., the change in impedance or current, not the absolute values) measured under identical assay conditions, ensuring that observed differences are attributable to the overall sensing platform rather than to the reference/counter electrode geometries.

**Table 1.** List of probes, targets, and primers.

oligonucleotide	Sequence (5' - 3')
<i>lytA</i> probe	[Thi1C6] [SP18] TGCCGAAAACGCTTGATACA
<i>lytA</i> target	TGTATCAAGCGTTTTTCGGCA
<i>lytA</i> Forward primer	TTGGGAACGGTTGCATCATG
<i>lytA</i> Reverse primer	TCGTGCGTTTTTAATTCCAGCT
<i>blaOXA-1</i> Forward primer	AACAGAAGCATGGCTCGAAA
<i>blaOXA-1</i> Reverse primer	TGGTGTTTTCTATGGCTGAGTT

### 2.3. Fabrication of a DNA biosensor

All experiments used the same protocol for probe functionalisation and a scheme is provided in **Figure 2A**. A solution mixture containing 3.0  $\mu\text{M}$  *lytA* probe solution and 15  $\mu\text{M}$  TCEP solution was first prepared. This mixture was applied to the PCB electrode cell surface and incubated overnight at room temperature. A PBS wash was then performed to remove any non-specifically bound DNA. The electrode surface was subsequently backfilled with 1.0 mM MCP for 1 h at room temperature, followed by another PBS wash to eliminate excess material. This process yielded the final *lytA* PCB biosensors. For a typical electrochemical measurement of *lytA* detection, target concentrations were sequentially incubated on the biosensor electrode



surface for 30 min at room temperature. After each incubation, the electrodes were washed with PBS to remove unbound material before measurement. This cycle was repeated for each concentration. The sequences of the *lytA* primers and probes were adopted from previous literature.<sup>19</sup> The blaOXA-1 (*oxa*) primers were designed in-house using the *E. coli* plasmid pEK499 genome sequence, based on methods described in previous studies.<sup>20</sup>

#### 2.4. Polymerase Chain Reaction (PCR) amplification

PCR amplifications were carried out using a miniPCR mini8 thermal cycler, and the resulting products were analysed using the blueGel electrophoresis system (miniPCR Bio, Cambridge, MA, USA) (**Figure 2B**). Quantification of PCR products was performed using a Qubit 4 Fluorometer (Thermo Fisher Scientific). The 235 bp *lytA* amplicons were amplified from *S. pneumoniae* genomic DNA TIGR4 [ATCC BAA-334] (LGC Standards, Middlesex, UK), while *oxa* amplicons were amplified from *E. coli* plasmid pEK499. Asymmetric PCR was achieved by lowering the concentration of the forward primer, resulting in an unequal amount of forward and reverse segments to hybridize, and thereby producing a higher concentration of single-stranded DNA (ssDNA) target amplicons. Asymmetric digoxigenin (DIG)-labelled amplification followed the same approach but used a DIG PCR mix (Sigma-Aldrich) in place of the standard mix, allowing incorporation of DIG into the amplified sequence. The DIG-labelled target was subsequently detected using horseradish peroxidase (HRP)-conjugated anti-digoxigenin antibody [HRP.21H8] (Abcam), which binds specifically to the DIG moiety. The bound HRP facilitates the oxidation of 3,3',5,5'-Tetramethylbenzidine (TMB), which can then be electrochemically reduced and quantified via chronoamperometry.

#### 2.5. PCR amplicons in PBS

Various types of 235 bp *lytA* PCR amplicons (positive control) and 115 bp *oxa* PCR amplicons (derived from OXA-48-type  $\beta$ -lactamase gene; negative control) were utilized in the experiments. The used amplicon types included, (1) standard PCR amplicons for *lytA* and *oxa*, which required preheating at 95°C for 5 min to denature the double-stranded DNA, (2) Asymmetric *lytA* and *oxa* PCR amplicons, which did not require heat treatment, and (3) Asymmetric DIG-labelled *lytA* and *oxa* PCR amplicons for electrochemical detection via antibody recognition. All amplicons were diluted in 1×PBS, and a range of target concentrations was tested. Target incubation was performed for 15 min at room temperature, followed by PBS and 0.05% Tween washing steps prior to measurement. For DIG-labelled PCR amplicons, chronoamperometric detection was carried out by incubating the electrodes



with anti-DIG antibodies (diluted 1:1000 from stock) for 30 min at room temperature. This was followed by a brief 20 s  $1\times$  PBS wash, after which 10  $\mu$ L of TMB substrate was added and allowed to react for 20 min. Chronoamperometry was then performed with an applied potential ( $E_{dc}$ ) of  $-0.15$  V for 2 s.

[View Article Online](#)

DOI: 10.1039/D3SD00210A

## 2.6. PCR amplicons in human serum

PCB P4 was used for all experiments given in this section. Standard *lytA* and *oxa* PCR amplicons were first denatured by heating at  $95^{\circ}\text{C}$  for 5 min to convert the double-stranded DNA into single strands. The denatured amplicons were then spiked into 100% human serum (origin: human male AB plasma, USA; sterile filtered, Sigma-Aldrich) to make various concentrations of target. Each concentration was sequentially incubated on the electrodes for 15 min at room temperature. After each incubation, the electrodes were washed with 0.05% Tween solution, tested, then rinsed with PBS before proceeding to the next target concentration. This process was repeated until all concentrations had been tested.

## 2.7. Electrochemical measurements:

Electrochemical measurements were performed using a PalmSens4 potentiostat running with PSTrace software (Alvatek electrochemical solutions, Houten, Netherlands). All measurements in this work were performed sequentially on individual working electrodes using a MUX8-R2 multiplexer. Measurements were performed in at least triplicate, and the averaged results were used for data analysis and calculations. Each PCB electrode utilised its inbuilt Au counter and reference electrodes. Unless otherwise specified in the figure captions, the redox buffer used for all measurements consisted of 2.0 mM  $\text{K}_3\text{Fe}(\text{CN})_6$  and 2.0 mM  $\text{K}_4\text{Fe}(\text{CN})_6$  prepared in  $0.5\times$ PBS. The measurement parameters for chronoamperometry (TMB-based): Applied potential ( $E_{dc}$ ) =  $-0.15$  V, duration = 2 s. Electrochemical impedance spectroscopy (EIS) parameters: DC bias potential = 0.0 V (vs. open-circuit potential); frequency range = 1 Hz to 50 kHz.



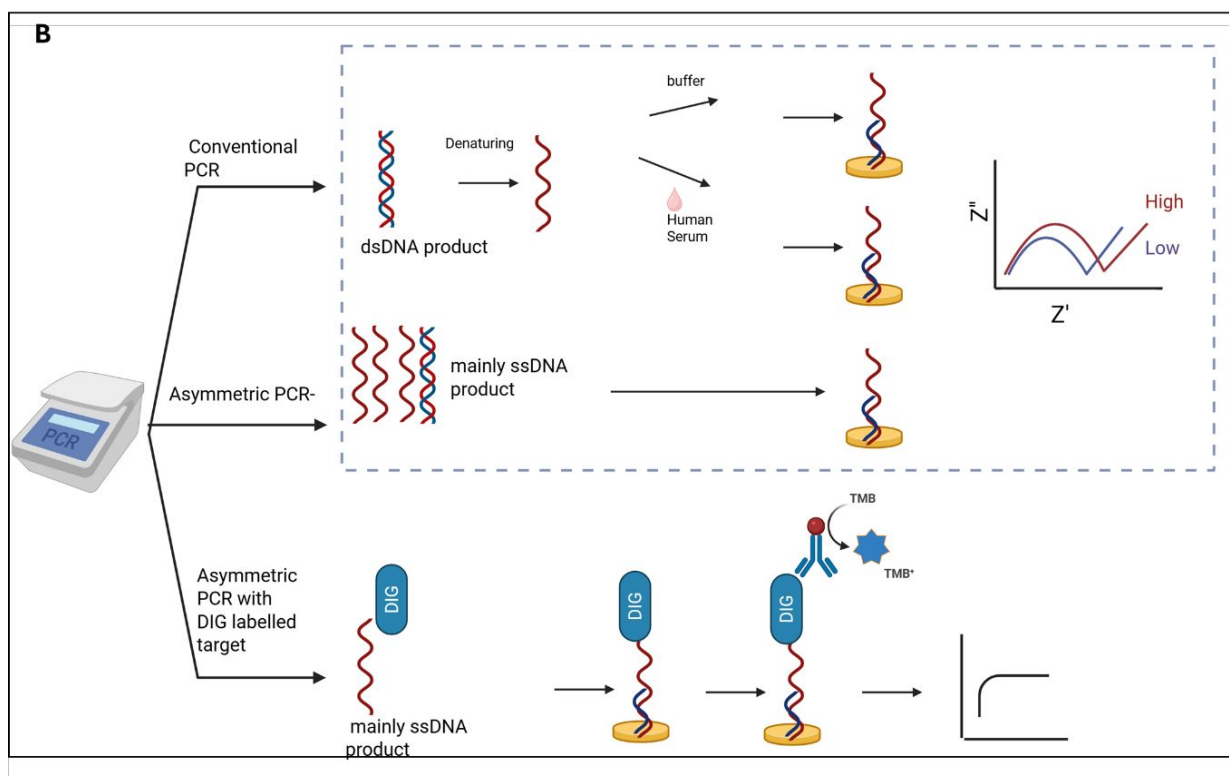
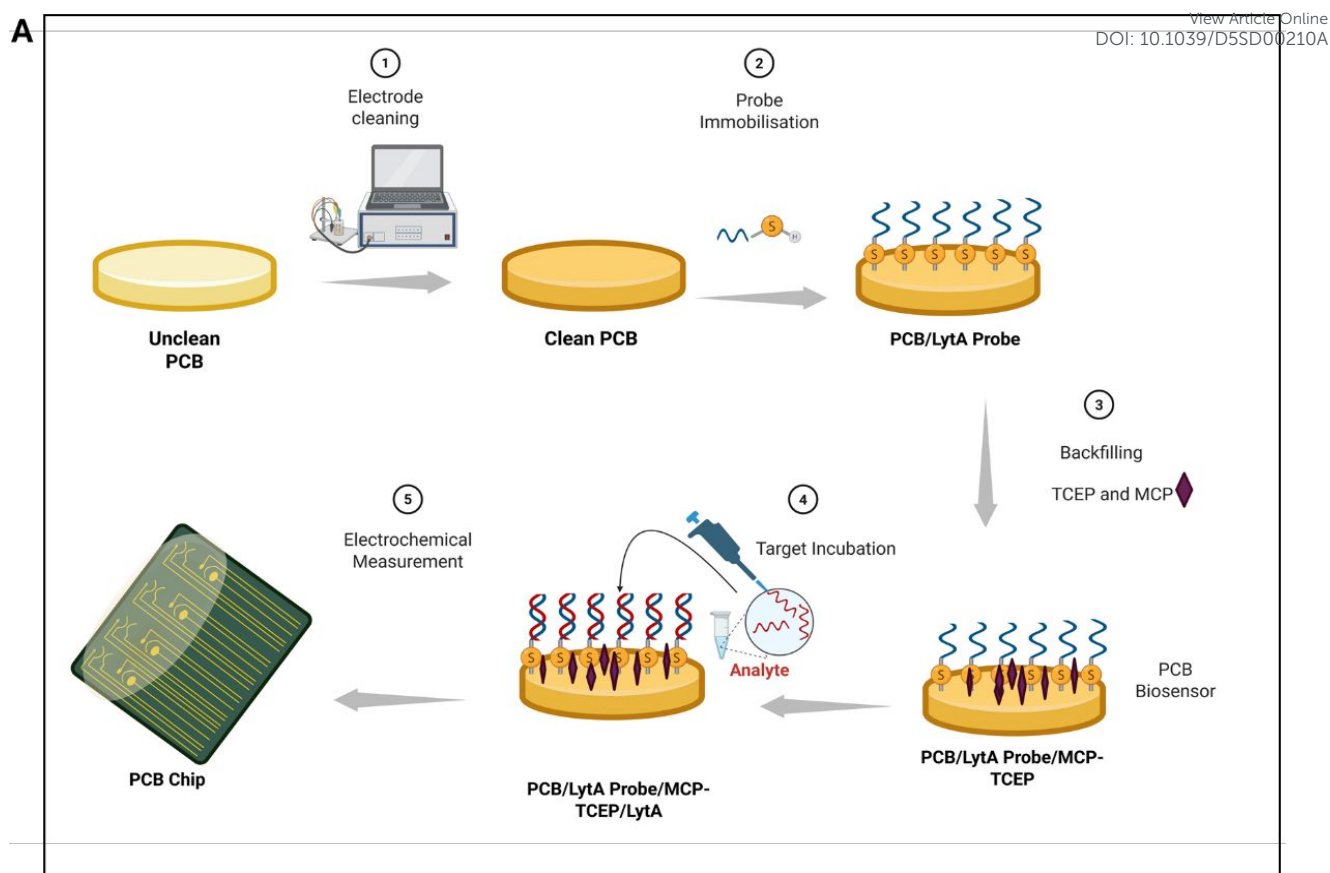


**Figure 2.** A) Biosensor fabrication scheme and sensor working principles: (1) Electrode cleaning, (2) probe immobilisation, (3) MCP backfilling, (4) Target immobilisation, (5)



Electrochemical measurements using PCB biosensors. B) Amplification procedures used in this work: conventional PCR, asymmetric PCR, and asymmetric PCR with DIG labelled target.

View Article Online  
DOI: 10.1039/D5SD00210A

### 3. Results and discussions

#### 3.1. Designing PCBs

The first PCBs designed in this work were designated PCB P1. It consisted of eight working electrodes of various diameters (**Table S1**), arranged around a central circular reference electrode and an annular counter electrode (**Figure 1A**) and were manufactured in-house. The objectives for this prototype were, (1) to assess whether the copper pads and traces could be successfully plated with gold, (2) to evaluate the ease and speed of interfacing the PCB with a potentiostat measurement system, and (3) to determine whether the Au surface capable of providing suitable electrochemical response that would justify further development for biosensing applications.<sup>21, 22</sup> PCB P1 incorporates multiple working electrodes with different diameters as part of a geometry exploration study. All working electrodes were used, they were just normalised by their area to make them comparable, and no mixing of data from different diameters occurred within a given analysis. Where comparisons were made across different working electrode geometries, current density and area-normalised impedance were used to ensure that the results were normalised to electrode area and therefore directly comparable despite geometric differences.

Next, commercially manufactured PCBs were purchased. The design was changed to include eight working electrodes of equal diameter and rectangular reference and counter electrodes, which generating a more spatially efficient layout (**Table S1**). Two versions of this updated design were obtained: (1) PCB P2, which was Au plated by the manufacturer, and (2) PCB P3, which was left non-plated to allow for in-lab testing of various Au plating techniques. Utilising a third-party manufacturer enabled the production of a larger number of devices and better quality of fabrication. Both PCB P2 and P3 exhibited electrochemical responses characteristic of Au surfaces. Notably, PCB P3 demonstrated superior electrochemical behaviour, although with limited reproducibility. Drawing from the insights gained through the development and testing of PCBs P1 to P3, a refined version was designed and commercially produced. This final electrode, offering optimal and reproducible performance, was designated as PCB P4.

Thus, the four PCB electrodes were selected to represent a progression of fabrication pathways relevant to biosensor development and scale-up: from in-house prototyping (P1) to



commercial manufacturing with varying levels of optimization (P2–P4). Their surfaces are inherently dissimilar due to differences in manufacturing processes, which directly influence surface properties such as roughness and active area. This variability allows for a practical comparison of how common fabrication choices impact electrochemical biosensing performance when tested under identical assay conditions. The goal of this comparison was to identify the manufacturing route that provides the optimal balance of sensitivity, reproducibility, and scalability for a low-cost diagnostic platform.

### 3.2. *lytA* detection using custom PCB electrodes

The *lytA* DNA detection performance of four PCB designs (P1–P4) was evaluated using differential pulse voltammetry (DPV) and EIS. All electrodes underwent identical self-assembled monolayer (SAM) functionalization, with measurements conducted in 5.0 mM redox buffer. DPV measurements were performed on all four PCB designs before and after incubation with 500 pM *lytA* target DNA. **Figure 3A** presents the DPV current densities, while **Figure 3B** shows the corresponding baseline-subtracted currents. PCB P1 exhibited a moderate current decrease (−44%) upon 1.0 nM *lytA* addition, though the target and control groups overlapped, indicating no significant differentiation. PCB P2 showed a 41.5% current increase at 1.0 μM *lytA* but similarly lacked statistical distinction from the SAM group. In contrast, PCB P3 demonstrated a pronounced current reduction (≈ 95%) at 500 pM *lytA*, with clear separation between target and control data without any overlap. However, it suffered from electrode loss (4 electrodes) and inconsistent performance. PCB P4 also displayed significant current decreases (≈ 26%) at 500 pM, with compacted distributions and no data overlap between groups. Two outliers were observed, but their inclusion did not alter the conclusion of distinct target/SAM responses. Notably, P4 initially lost two electrodes due to a connector issue (unrelated to the electrodes themselves), which was resolved in subsequent experiments. **Figures 3C** present the charge transfer resistance ( $R_{ct}$ ) values from EIS measurements before and after incubation with 500 pM *lytA* target DNA addition for each PCB electrode and **Figure 3D** presents the corresponding percentage changes. PCB P1 showed a minor  $R_{ct}$  decrease reduction (−8.6%), with overlapping distributions indicating no significant difference. PCB P2 exhibited minimal impedance values and a 76.6% increase, though not discernible from DPV data due to axis scaling; no statistical distinction was found. P3 produced unreliable EIS fits, precluding analysis. In contrast, PCB P4 demonstrated a clear 211% increase in impedance, with non-overlapping data ranges suggesting reliable target detection.



Overall, PCB P1 and P2 failed to demonstrate reliable *lytA* detection. PCB P3 showed promising DPV performance but suffered from inconsistent EIS results and electrode loss. PCB P4 outperformed all other designs, offering robust and reproducible detection of 500 pM *lytA* using both DPV and EIS, with improved electrode consistency following connector repair. Based on its superior sensing performance, stability, and reliability, PCB P4 was selected for all subsequent biosensing experiments.

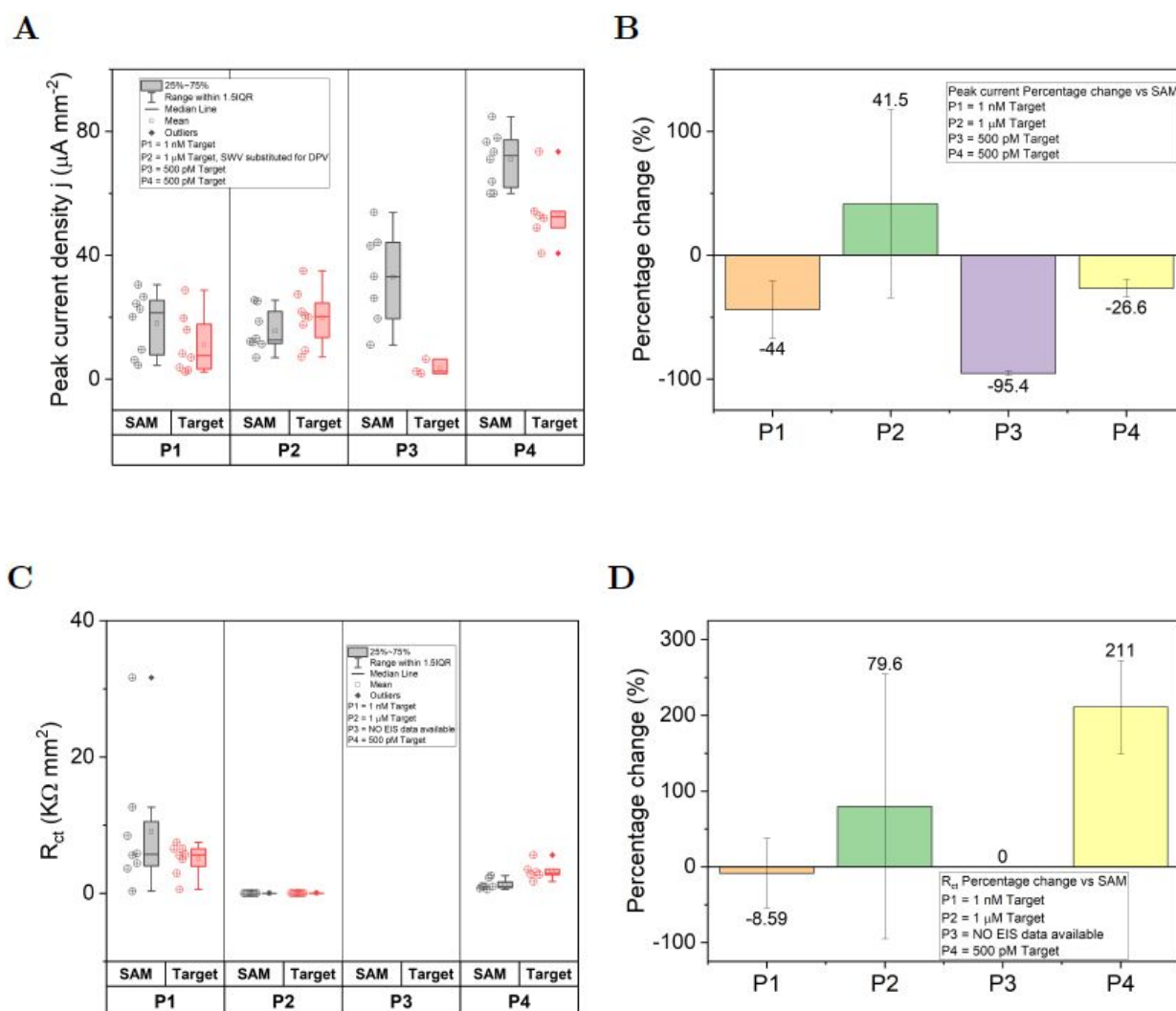


**Figure 3.** Performance comparison of four PCB designs (P1-P4) for *lytA* detection. (A) DPV current density for each PCB electrode after SAM formation (control) and after incubation with 500 pM *lytA* target DNA and, (B) Corresponding percentage change in DPV peak current for each PCB type upon target addition. (C) Charge transfer resistance ( $R_{ct}$ ) values from EIS measurements for each PCB after SAM formation and after incubation with 500 pM *lytA* target, and (D) Corresponding percentage change in  $R_{ct}$  for each PCB type upon target



addition. All measurements were performed in 5.0 mM redox buffer. Data points represent individual replicates ( $n = 8$ ).

View Article Online  
DOI: 10.1039/C5SD00210A

### 3.3. Detailed investigation of *lytA* detection using PCB P4

The performance of PCB P4 for detecting various concentrations of *lytA* target DNA was evaluated, and the results are presented in **Figure 4**. The DPV response current was linearly decreased and showed a dose-dependent fashion for different concentration range of target from 500 fM to 500 nM. The mean percentage change in DPV peak current demonstrated a generally linear and dose-dependent decrease in response to increasing *lytA* concentrations. However, the 5.0 pM concentration slightly deviated from this trend, and a trend reversal was observed at 50 pM, after which the signal continued to decrease with higher concentrations (**Figure 4A**). This unexpected trend reversal most likely occurred due to the multiple incubations, washes and testing that destabilising the probe DNA. The corresponding raw DPV peak current data showed considerable spread, with significant differences likely occurring between the SAM control and the 30 pM to 50 nM target concentrations; the remaining concentrations appeared statistically similar (**Figure 4B**). Square wave voltammetry (SWV) results exhibited comparable percentage change magnitudes and dose-response trends across a range of 500 fM to 500 nM (**Figure 4C**), with the raw data reflecting similar behaviour to DPV but with fewer outliers (**Figure 4D**). Likely significant differences between the SAM control and target samples were again observed in the 30 pM to 50 nM range. The mean  $R_{ct}$  percentage change from the EIS results were also showed a dose-dependent increase, with the 5.0 pM concentration again deviating from the overall trend and a noticeable reversal at 50 pM, consistent with the DPV and SWV results (**Figure 4E**). Notably, the magnitude of the EIS response was significantly larger, about 250% compared to the ~ 30% observed with DPV and SWV. The raw  $R_{ct}$  data showed several outliers; exclusion of these would have reduced the magnitude of the percentage change but improved statistical errors ((**Figure 4F**). Significant differences between the SAM control and the target DNA were evident from 10 pM up to 50 nM. Overall, EIS was found to be the best performing detection technique among the CV, SWV and EIS, demonstrating the highest magnitude of percentage changes, clearer distinctions between control and target stages, and smaller data spreads for each concentration of *lytA*.



Further analysis of *lytA* detection performance on PCB P4 was conducted by performing linear regression within the linear response region between 10 pM and 50 pM. The LoD was also calculated. The LoD for *lytA* was determined to be 10.4 pM, 12.39 pM, and 4.5 pM using DPV, SWV, and EIS, respectively. A second linear response region was observed in all three techniques, between 0 and 2.0 pM, yielding LOD values ranging from 251 to 433 fM. This suggests that the PCB P4 biosensor is capable of detecting femtomolar concentrations of 20 bp complementary *S. pneumoniae* DNA, indicating potential for ultra-sensitive detection. Notably, a previously reported Peptide Nucleic Acid (PNA)-based PCB device for rapid and high-sensitivity DNA quantification reported an LoD of 57 fM.<sup>17</sup> The biosensor described in this work demonstrated comparable LoDs (251–433 fM) without requiring expensive PNA reagents, instead relying on a straightforward SAM modification strategy.

View Article Online  
DOI: 10.1059/DS3D00210A



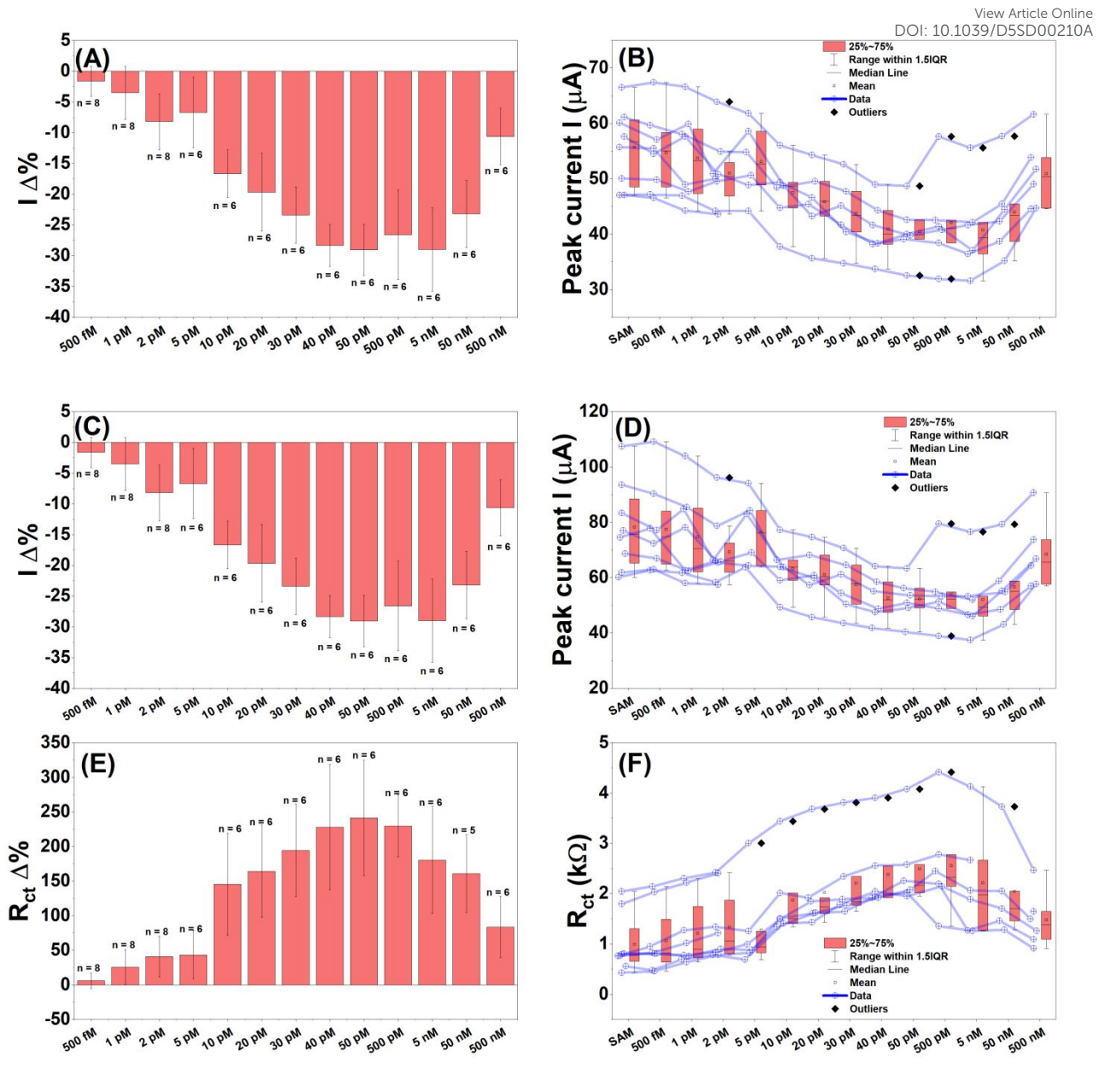


**Figure 4.** Concentration-dependent detection of the 20 bp *lytA* target using PCB P4. (A) Mean percentage change in DPV peak current across target concentrations (500 fM to 500 nM) and (B) corresponding raw DPV peak current values at each concentration. (C) Mean percentage change in SWV peak current across different target concentrations (500 fM to 500 nM) and (D) corresponding raw SWV peak current values at each concentration. (E) Mean percentage change in  $R_{ct}$  from EIS measurements and (F) corresponding raw  $R_{ct}$  values at each concentration. All measurements were performed in 5.0 mM redox buffer. Sample size  $n=5-8$ .

### 3.4. PCR amplification of genetic sequences at PCB P4



With a suitable platform established and successful detection of the 20 bp complementary *lytA* DNA sequences in PBS, the performance of the probe was next subjected to longer DNA target fragments. This aimed to more precisely replicate the DNA lengths that a sensor would be required to deal with in a PoC settings. For this purpose, a 235 bp sequence (amplified from *S. pneumoniae* genomic DNA) that contained the 20 bp *lytA* complementary sequence in the middle of this larger sequence. The reason for it being in the middle and not at the ends of the sequence was due to the primer design from the previous literature.<sup>19</sup> To further validate the specificity of the *lytA* probe, negative controls were included using 115 bp *oxa* amplicons.

### 3.4.1. *lytA* 235 bp and *oxa* 115 bp PCR amplification

The PCR amplification of the 235 bp *lytA* target was first assessed using a Qubit 4 fluorometer, and the results are given in **Table 2**. The positive amplified *lytA* PCR mixture yielded a concentration of 14.1 µg/mL, while the negative control (without genomic DNA template) showed only 0.9 µg/mL. This clear difference confirmed successful amplification in the positive sample. This quantification confirmed the presence of amplified nucleic acid but could not verify whether it was the desired *lytA* DNA sequence. To confirm the specificity of the amplification, an electrophoresis gel was performed on both positive and negative PCR products (**Figure S3A**). The negative control showed no visible band, indicating that no significant amplification occurred. In contrast, a visible band in the positive lane was observed between the 200 bp – 300 bp on the reference ladder, confirming the amplification of a product consistent with the desired 235 bp *lytA* amplicon.

Similarly, for the *oxa* amplifications, the positive PCR mixture showed a concentration of 11.3 µg/mL, while the negative control measured 2.78 µg/mL (**Table 2**). The significantly higher concentration in the positive sample confirmed successful nucleic acid amplification. The electrophoresis gel analysis revealed no visible band in the negative lane, while the positive lane showed a clear band in the lower end in the range of 100–200 bp (**Figure S3B**), consistent with the desired sequence of 115 bp long amplicon. The distorted appearance of the gel was noted, which could be attributed to water vapour condensation on the plastic cover. These results confirmed successful amplification of the *oxa* amplicons, enabling the subsequent specificity testing.

**Table 2.** List of PCR amplifications



S.No.	Amplifying Target	Length (bp)	Qubit Quantification ( $\mu\text{g/mL}$ )
1.	<i>lytA</i> ( <i>S. pneumoniae</i> )		
	Positive	235	14.1
	Negative	NA	0.9
2.	<i>lytA</i> ( <i>S. pneumoniae</i> ) DIG		
	Positive	235	3.29
	Negative	NA	2.57
3.	<i>lytA</i> ( <i>S. pneumoniae</i> ) Asymmetric		
	Positive	235	6.73
	Negative	NA	0.399
4.	<i>lytA</i> ( <i>S. pneumoniae</i> ) Asymmetric DIG		
	Positive	235	8.73
	Negative	NA	1.11
5.	<i>oxa</i> ( <i>E. coli</i> )		
	Positive	115	11.3
	Negative	NA	2.78
6.	<i>oxa</i> ( <i>E. coli</i> ) DIG		
	Positive	115	4.89
	Negative	NA	2.75
7.	<i>oxa</i> ( <i>E. coli</i> ) Asymmetric		
	Positive	115	5.13
	Negative	NA	2.16
8.	<i>oxa</i> ( <i>E. coli</i> ) Asymmetric DIG		
	Positive	115	46.4
	Negative	NA	2.23

### 3.4.2. Asymmetric and asymmetric DIG-labelled *lytA* and OXA PCR amplification



The PCR amplifications of DIG-labelled *lytA* and *oxa*, as well as asymmetric *oxa*, did not attain successful quantification results (**Table 2**). Positive samples showed relatively lower concentrations, while negative controls showed higher values. However, asymmetric DIG-labelled *oxa* displayed notably high amplification (46.4  $\mu\text{g/mL}$ ), with its corresponding negative showing a low concentration, indicating successful amplification. Electrophoresis gels of these samples revealed that all *lytA* samples (both DIG-labelled and unlabelled) failed to show bands in either the positive or negative lanes (**Figure S3C**). DIG-labelled *oxa* showed bands in both the positive and negative lanes, indicating possible contamination in the negative control. Asymmetric *oxa* showed no visible bands, while asymmetric DIG-labelled *oxa* displayed a band in the positive lane but not in the negative. The inconsistent behaviour observed in the gel, particularly the presence or absence of bands, may have resulted from pipetting errors or sample misloading, leading to inconclusive electrophoresis outcomes. Despite the inconclusive gel results, Qubit quantification indicated the likely presence of amplicons in several of these samples. Therefore, experiments using these PCR products proceeded, with subsequent biosensing results potentially serving to validate the success of the amplifications.

### 3.5. *lytA* genetic amplicons in PBS using PCB P4

#### 3.5.1. Detection of 235 bp *lytA* amplicons in PBS

The 235 bp *lytA* amplicon was diluted in PBS to prepare a range of target concentrations (1.0 pM to 100 pM). Prior to electrode incubation, the DNA solutions were denatured at 95°C for 5 min to ensure single-stranded DNA, then transferred to the electrode surfaces and incubated for 15 min. Although the mean DPV percentage change initially increased with target concentration, it subsequently showed a gradual decline (**Figure 5A**). However, no clear dose-dependent trend was observed, and the results were marked by overlapping error bars. The raw DPV current data confirmed this, showing no statistically significant differences between the control and target stages (**Figure 5B**). Similar results were observed with SWV for the same concentration range (1.0 pM to 100 pM), where the percentage changes lacked a clear dose response and were accompanied by overlapping errors (**Figure 5C**). The initial response was found to decrease, however, contrary to the DPV behaviour, remained that way for all target concentrations. There appeared to be an absence of differences between SAM and target stages, with the introduction of more outliers (**Figure 5D**). EIS delivered the most promising results. The mean  $R_{ct}$  percentage change showed a dose-dependent increase from 1.0 pM to 50 pM,



with a trend reversal phenomenon appearing again at 50 pM (**Figure 5E**). Although the  $R_{ct}$  data for the target stages exhibited wide variability, the SAM stage had a narrower spread, enabling likely differentiation between the SAM and target stages in the 20–50 pM range (**Figure 5F**). These EIS results confirmed the successful detection of the 235 bp *lytA* amplicons in PBS using PCB P4 electrode.

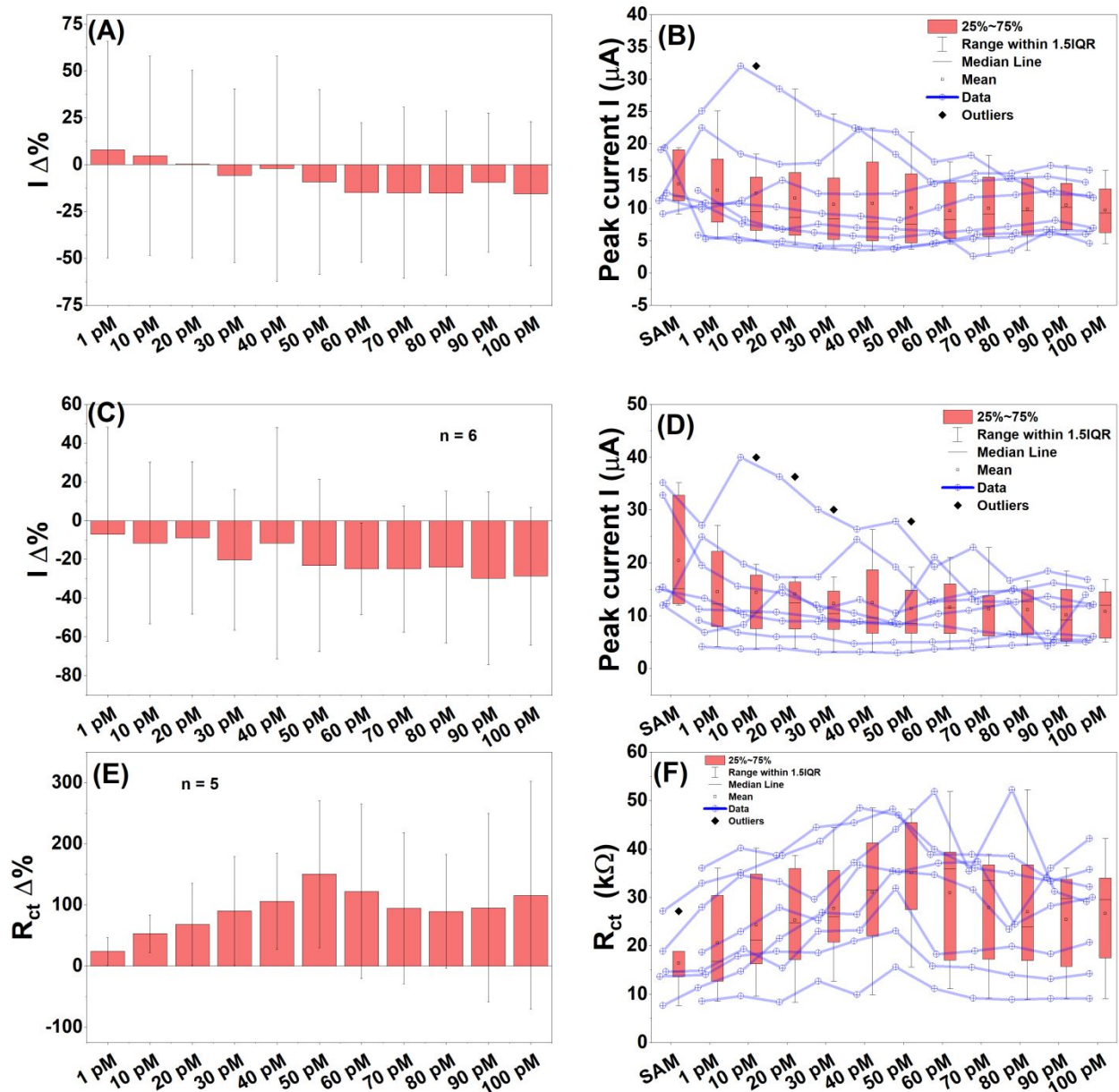


**Figure 5.** Detection of *lytA* 235 bp PCB amplicons in PBC using PCB P4. (A) Mean percentage change in DPV peak current for target concentrations ranging from 1.0 pM to 100 pM, and (B) Corresponding raw DPV peak current values. (C) Mean percentage change in SWV peak current for various target concentrations and (D) Corresponding raw SWV peak current values. (E) Mean percentage change in  $R_{ct}$  from EIS measurement for various target concentrations.



(F) Corresponding raw  $R_{ct}$  values. All measurements were conducted using a ferri/ferrocyanide redox buffer.  $n = 8$ .

View Article Online  
DOI: 10.1039/D5SD00210A

### 3.5.2. Asymmetric *lytA* and *oxa* amplicons in PBS

The asymmetric PCR amplicons were incubated on separate PCBs (positive and negative) for 15 min in PBS. Heating was not required, as the asymmetric reaction is expected to produce single-stranded DNA directly suitable for sensor interaction. The mean DPV percentage changes displayed a decreasing dose-dependent response with increasing concentrations of the positive (*lytA*) amplicon target concentrations from 1.0 pM to 100 pM (**Figure 6A**). The negative control (*oxa*) also showed a dose-dependent response and produced a slightly higher response than the positive. The normalised DPV data confirmed the absence of statistically significant differences between the *lytA* and *oxa* responses (**Figure 6B**), though the data spread and associated errors were improved compared to the first amplicon experiment. The SWV response was similar to DPV results, showing comparable dose responses for both control groups (**Figure 6C**), but with a greater magnitude of percentage change. Notably, potential significant differences between the positive and negative groups were observed at 20 pM and 40 pM (**Figure 6D**), suggesting that the negative amplicon generated a stronger response than the positive, which was an unexpected result. EIS results also revealed dose-dependent trends in both control groups, with the negative showing a greater response overall (**Figure 6E**). The data was affected by large errors in some stages, particularly in the positive and most negative conditions. Normalised  $R_{ct}$  data indicated that these large variances could largely be attributed to a single outlier electrode; when excluded, the data showed potential significant differences at 20 pM and 60 pM (**Figure 6F**). However, the outlier was retained in the percentage change data for full transparency, serving as a reminder that improved error margins could be achieved by statistically rejecting such anomalous data points.

These results can likely be attributed to non-specific biofouling of the electrode surface. As shown in **Table 2**, both asymmetric *lytA* and *oxa* reactions produced similar levels of amplified material (6.73 and 5.13  $\mu\text{g/mL}$ , respectively). However, the electrophoresis gel analysis for both showed no indication of bands in their lanes which suggested that the specific DNA material was not present in the sample. If this were true, then both PCBs exposed to the *lytA* positive and *oxa* negative were in reality receiving various concentrations of non-specific proteins and nucleotide mixtures that composed the PCR solutions. The responses seen here



would then easily be explained as a biofouling dose response of these protein/nucleotide contaminants with none or insufficient quantities of amplicons present.

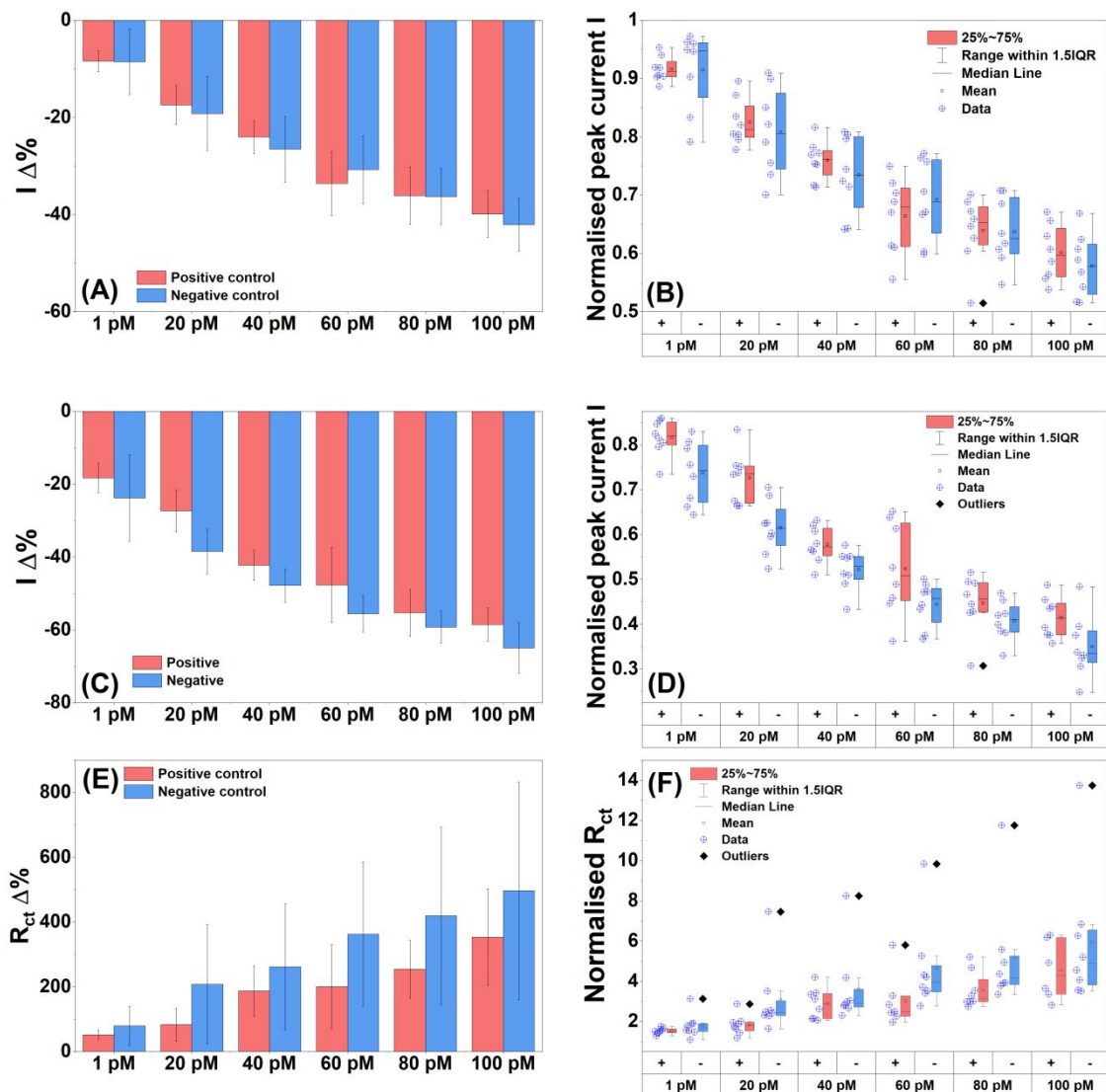


**Figure 6.** Detection of asymmetric *lytA* 235 bp amplicons in PBS using PCB P4. (A) Mean percentage change in DPV peak current for target concentration ranging from 1.0 pM to 100 pM and (B) corresponding raw DPV peak current values. (C) Mean percentage change in SWV peak current across various target concentrations (1.0 pM to 100 pM) and (D) corresponding raw SWV peak current values. (E) Mean percentage change in  $R_{ct}$  from EIS measurements for various target concentrations (1.0 pM to 100 pM) and (F) Corresponding raw  $R_{ct}$  data.  $n = 8$ .

### 3.5.3. Asymmetric DIG-labelled *lytA* and *oxa* amplicons in PBS



About 40 pM positive and negative amplicons were incubated on the electrodes for 15 min at 50°C, followed by washing and subsequent incubation with HRP tagged anti-DIG antibody at room temperature for 30 min. The mean DPV percentage change showed that both controls had decreased current change (**Figure S4A**). The positive decreased more than the negative -40% vs -10 %. The normalised DPV peak currents confirmed this behaviour resulting in a likely difference between the controls demonstrating successful specific detection of 40 pM asymmetric DIG-labelled *lytA* DNA (**Figure S4B**). Mean  $R_{ct}$  percentage change showed an increase in response target 100% vs 40% (**Figure S4C**). The normalised  $R_{ct}$  data supported this and was on the verge of a likely difference (**Figure S4D**).

The PCBs were washed after the previous measurements and TMB was applied for 20 min. The TMB solution turned blue confirming the presences of HRP. Chronoamperometry was performed producing a current decrease for both positive and negative controls (**Figure 6 S4E**, Test 1). There were no differences between the controls. To ensure that the unspecifically bound HRP was properly removed a second wash incorporating 20 s of 1 x PBS, 20 s of 0.05 % tween, and then 20 s of 0.1 x PBS was performed and reapplication of TMB for 20 min was undertaken. The response again showed a current decrease for both controls with the negative decreasing more than the positive (**Figure S4E**, Test 2) producing no differences between the groups. This chronoamperometry method produced TMB colour reactions for both control groups solutions when only the positive control should. This meant that the HRP anti DIG antibodies were present on the negative control and were unspecifically bound, with multiple washing attempts unable to successfully remove them.

### 3.6. *lytA* genetic amplicon in human serum

With successful specific detection of full complementary 20 bp and 235 bp normal PCR and asymmetric DIG-labelled amplicons in PBS, the next step was to attempt detection of the 235 bp amplicon (amplified from *S. pneumoniae* genomic DNA) in a clinically relevant matrix. Normal 235 bp *lytA* and 115 bp *oxa* PCR product was heated to 95°C for 5 min and then spiked into 100% human serum. The serum samples were incubated on the electrode surface for 15 min, tween washed and then tested. The target concentration range was 1.0 pM to 100 pM. The mean DPV peak current percentage change displayed a dose dependant response to increasing target with 20 pM failing to follow the trend (**Figure 7A**). The negative control also showed a dose-dependent response. The normalised DPV data confirmed the percentage changes with the 20 pM verging on a likely difference between the two controls (**Figure 7B**). The other



target concentrations showed no differences. The mean SWV peak current percentage changes showed a slight improvement over DPV with more pronounced differences between control groups (**Figure 7C**). Dose dependence was again present for both control groups. The normalised data showed that 1.0 and 20 pM control groups were likely different and 60, 80 and 100 pM were close to being different (**Figure 7D**).

EIS again proved to be the best performing detection techniques with PCB P4 biosensor. The mean  $R_{ct}$  percentage change showed increasing dose dependence for the positive control (**Figure 7E**). The negative control increased until 40 pM then remained constant until 100 pM where it then increased slightly. Therefore, the negative control did not produce a strong dose response, and the sensor demonstrated anti-biofouling properties. The normalised mean  $R_{ct}$  data showed likely differences between positive and negative groups for 1.0, 60, 80 and 100 pM (**Figure 7F**). Some positive target stages were likely different from each other indicating a strong signal response to target DNA while no differences were found within the negative control group, meaning they were all likely equivalent further reinforcing the anti-biofouling performance of the sensor. The LoD values for the various measurement techniques were calculated, which were 23 pM for DPV, 30 pM for SWV, and 18 pM for EIS. The LoD values correlated with the concentrations demonstrated to have likely differences from the box plot data, with the exception of EIS which was able to successfully detect target DNA at 1.0 pM which was significantly lower than the calculated LoD.

View Article Online  
DOI: 10.1039/C5SD00210A



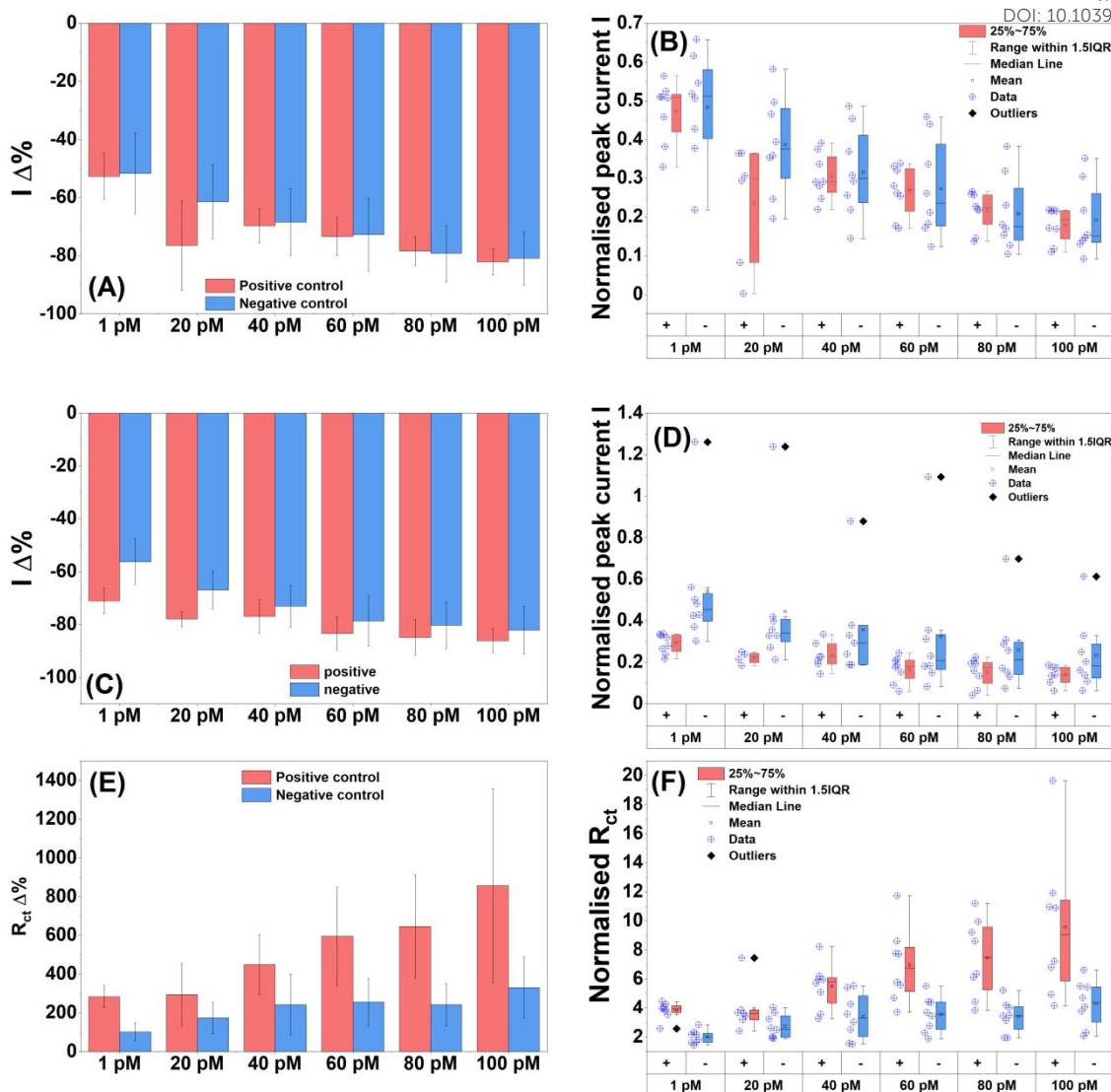


**Figure 7.** Detection of PCR amplicons in 100% human serum (*lytA* 235 bp (positive control) vs *oxa* 115 bp (negative control)) using PCB P4. (A) Mean percentage change in DPV peak current for *lytA* (235 bp) and *oxa* (115 bp, negative control) targets across a concentration range of 1.0 pM to 100 pM and (B) corresponding normalised DPV current values. (C) Mean percentage change in SWV peak current for *lytA* and *oxa* over a concentration range of 1.0 pM to 100 pM and (D) corresponding normalised SWV current values. (E) Mean percentage change in  $R_{ct}$  from EIS measurements for different concentration of positive and negative controls over a range of 1.0 pM to 100 pM and (F) corresponding normalised  $R_{ct}$  values. All measurements were conducted in a 2.0 mM ferri/ferrocyanide redox buffer.  $n = 8$ .

**Table 3** summarises the comparisons with sensors from literature. Compared to several previous sensors, the developed sensor demonstrated excellent responses for such a simple device and would hopefully continue showing such responses with testing of reduced



concentrations and incubation times. This is a vast improvement on current culture methods which regularly return no culture positive after multiple hours of incubation. This sensor also outperforms the pneumococcal urinary antigen test in terms of time to result, expense and complexity. The time to result are both 15 min but this should be easily reduced on this sensor system. The sensor does not require to be at specific temperature nor do the sample and reagents.<sup>11</sup> This sensor comprises of sample addition, wash, redox addition and then result, reducing the complexity of the assay. The antigen test requires sample and multiple reagents. Antigen tests are relatively expensive approximately in £3 – £5 whereas this sensor would likely be in the region of pence if it aligns its manufacture protocol with that of glucose strip production which is demonstrated in the next section for a Coronavirus Disease 2019 (COVID-19) sensor. Other tests on the market include a magnetogenosensor assay for *lytA* that was able to obtain a LoD of 1100 pM.<sup>19</sup> Other examples of reported *S. pneumoniae* sensors include a DNA-Antibody nanostructure assay ( $\approx 3.26$  pM),<sup>23</sup> polymer based genosensor ( $\approx 1 \times 10^6$  pM),<sup>24</sup> synergism strategy for gene sequence sensing (0.0005 pM),<sup>25</sup> and versatile loop-mediated isothermal amplification with a sensitivity of 0.173 pM.<sup>26</sup> The sensor developed in this work demonstrated similar or improved sensitivity to the devices reported. It was also able to achieve this in complex human serum with reduced time to result utilising less complicated functionalisation strategies on an easily manufacturable device. The sensors above that demonstrate low pM detection used complex devices, materials and methods to achieve this. The PCB P4 design, which provides a dedicated counter and reference electrode for each working electrode, creates an array of independent electrochemical cells. This design inherently minimizes the risk of crosstalk, a significant advantage for future parallelized operation in a point-of-care device.

For deployment as a practical PoC device, this PCB electrodes can be integrated into a single-use, disposable cartridge designed for 'plug-and-play' operation. Our group recently demonstrated a similar a plug-and-play, easy-to-manufacture PoC device for diagnostic applications.<sup>27</sup> Such cartridge houses can protect the delicate electrodes and electrical contacts, incorporates a defined sample chamber with a simple injection port for regulated sample introduction, and ensures robust fluidic containment to prevent user exposure to the sample or reagents. The user would simply inject the prepared sample, insert the cartridge into a portable, handheld reader, and receive a digital readout. This approach, common in commercial glucose meters and other POC diagnostics, effectively decouples the complex microfluidics and



electrochemistry from the end-user, ensuring reliability, safety, and ease of use. Future work will focus on prototyping such cartridges and integrating them with low-cost, portable readers. View Article Online  
DOI: 10.1039/D5SD00210A

For translation to a field-deployable POC device, power consumption is a key practical consideration. The electrochemical techniques employed (EIS, DPV) require very low operating currents (< 100  $\mu$ A). Commercial mini-potentiostats demonstrate that such systems can run for extended periods on small batteries or a smartphone connection.<sup>28, 29</sup> Therefore, a dedicated reader for this PCB platform would have minimal power demands, easily supporting a full day of operation on a compact, rechargeable battery, aligning with the requirements for use in resource-limited settings.

**Table 3.** Table of comparisons of *S pneumoniae* sensors.

Sensor/Technology	Label Free?	Approx. Cost per Test	Key Complexity	LOD (pM)	Time to Result	Real Sample
Cell culture	Yes	Low	Simple (but slow)	NA	72 h	Blood
PCR	Yes	High	Moderate	NA	Hours	Extracted DNA
UAT <sup>30</sup>	Yes	≈ £5	Moderate	NA	15 min	Urine
Magnetosensor <sup>19</sup>	No	High (~£4.65)	High (MB modification)	1100	5 h	Buffer
DNA antibody <sup>23</sup>	No	Very high	Very high (DNA tetrahedron)	3.26	>30 min	Serum
Polymer genosensor <sup>24</sup>	Yes	High	Moderate	$1 \times 10^6$	20 min @ 55°C	Buffer
Synergism gene sequence <sup>25</sup>	No	Very high	High (multiple probes)	0.0005	20–60 min	50% serum
LAMP <sup>26</sup>	No	Moderate (≈ £2.80)	High (microfluidics)	0.173	≈ 2 h	Clinical samples
PNA-based Lab-on-PCB <sup>17</sup>	Yes	Moderate (PNA costly)	High (microfluidics)	0.057	5 min (flow)	Buffer
<b>PCB electrodes (This work)</b>	<b>Yes</b>	<b>Very low (≈ £0.2)</b>	<b>Low (standard SAM)</b>	<b>1.0</b>	<b>15 min</b>	<b>100% serum</b>

Abbreviations: UAT: Urinary Antigen Test; LAMP: Loop-mediated isothermal amplification; PNA: Peptide nucleic acid; MB = Magnetic beads.



These results demonstrated that SWV could partially, and EIS could fully successfully and specifically detect an unlabelled 235 bp *lytA* amplicon amplified from *S. pneumoniae* full genomic DNA over a range of concentrations from 1.0-100 pM in 15 min at room temperature. Clinically relevant blood levels that can result in life-threatening infections can be as low as 1–10 colony-forming units per millilitre of blood (cfu/mL).<sup>31</sup> This equates to approximately attomolar (aM) levels of genetic material for detection. The sensor had shown possible femtomolar LoDs and should comfortably be able to detect these femtomolar concentrations. Attomolar ranges would be a challenge to achieve nevertheless until the sensor is tested with these concentrations no feasibility conclusions can be made. If the sensor was unable demonstrate detection at these small concentrations, then PCR amplification would have to be employed to amplify the DNA to detectable levels. This would be easily accomplished as PCR amplification was already employed for target sequence production for these experiments. Therefore, the infrastructure already existed and had been successfully demonstrated. Two hours of amplification were required to produce nanomolar levels of target DNA with the sensor demonstrating picomolar capabilities. Consequently, the attomolar DNA would only require amplification to picomolar levels shortening the current amplification times used. This would result in the successful detection of clinically relevant levels of *S. pneumoniae* in under 2 h.

#### 4. Conclusions

This study systematically investigated PCB-based electrodes for rapid sepsis diagnostics through *S. pneumoniae lytA* DNA detection. While prototype PCBs (P1-P3) showed progressive improvements in electrochemical performance, they faced limitations in reliability and consistency. The commercially fabricated PCB P4 emerged as the optimal platform, demonstrating superior and reproducible DNA detection capabilities, making it ideal for sepsis biosensor development. Using a 20 bp *lytA* sequence, we established an PCB P4 based electrochemical detection system with a 4.5 pM LoD in PBS. The system was further validated with PCR-amplified longer target sequences that successfully detects, normal double-stranded DNA amplicons, asymmetric (single-stranded DNA), asymmetric DIG-labelled amplicons, and 235 bp *lytA* sequences spiked in 100% human serum (1-100 pM detection via EIS in 15 min at room temperature). While some asymmetric PCR products showed detection limitations due to potential quantity/contamination issues, the platform demonstrated clinically relevant sensitivity. This work presents a functional biosensor capable of detecting 1.0 pM *lytA* amplicons in complex matrices within 15 minutes at ambient temperature. With further



optimization, this system shows strong potential for, reduced detection times, enhanced sensitivity, and direct clinical sample analysis. The developed PCB platform establishes a foundation for rapid, point-of-care sepsis diagnostics with significant translational promise.

View Article Online

DOI: 10.1039/D3SD00210A

### Conflicts of interest

The authors declare no conflict of interest.

### Data availability

Key data that supporting the findings of this study have been included in the manuscript. Additional data that supporting this article have been included as part of the Supplementary Information.

### Acknowledgements

This work was supported by the Centre for Advanced Measurement Science and Health Translation, University of Strathclyde. PAH would like to acknowledge the Royal Academy of Engineering Research Chair Scheme for long term personal research support (RCSRF2021\11\15). DA would like acknowledge educational support from Baxter Pharmaceuticals and MSD (Merck Sharp and Dohme). DC would like to thank the Dowager Countess Eleanor Peel Trust and Tenovus Scotland for seed grants in the area of sepsis monitoring. VV's EngD studentship was funded by the EPSRC CDT in Biomedical Devices and Health Technologies (EP/L015595/1).

### References

1. J.-L. Vincent, *EBioMedicine*, 2022, **86**.
2. T. K. Burki, *The Lancet Respiratory Medicine*, 2018, **6**, 826.
3. C. F. Duncan, T. Youngstein, M. D. Kirrane and D. O. Lonsdale, *Current infectious disease reports*, 2021, **23**, 1-14.
4. I. Martin-Loeches, L. F. Reyes and A. Rodriguez, *Thorax*, 2025.
5. N. Gopal, N. Chauhan, U. Jain, S. K. Dass, H. S. Sharma and R. Chandra, *Artificial Cells, Nanomedicine, and Biotechnology*, 2023, **51**, 476-490.



6. A. S. Tanak, A. Sardesai, S. Muthukumar and S. Prasad, *Bioengineering & Translational Medicine*, 2022, **7**, e10310. New Article Online  
DOI: 10.1039/D5SD00210A
7. S. Balayan, N. Chauhan, R. Chandra, N. K. Kuchhal and U. Jain, *Biosensors and Bioelectronics*, 2020, **169**, 112552.
8. R. Varghese, R. Jayaraman and B. Veeraraghavan, *Journal of microbiological methods*, 2017, **141**, 48-54.
9. S. L. Goh, B. P. Kee, K. Abdul Jabar, K. H. Chua, A. M. Nathan, J. Bruyne, S. T. Ngoi and C. S. J. Teh, *Pathogens and Global Health*, 2020, **114**, 46-54.
10. W.-T. Fan, T.-T. Qin, R.-R. Bi, H.-Q. Kang, P. Ma and B. Gu, *European Journal of Clinical Microbiology & Infectious Diseases*, 2017, **36**, 1005-1012.
11. P. Kim, A. Deshpande and M. B. Rothberg, *Infection and drug resistance*, 2022, 2219-2228.
12. B. Kim, J. Kim, Y. H. Jo, J. H. Lee, J. E. Hwang, M. J. Park and S. Lee, *Plos One*, 2018, **13**, e0200620.
13. P. Lasserre, B. Balansethupathy, V. J. Vezza, A. Butterworth, A. Macdonald, E. O. Blair, L. McAteer, S. Hannah, A. C. Ward and P. A. Hoskisson, *Analytical chemistry*, 2022, **94**, 2126-2133.
14. S. Kumar, S. Tripathy, A. Jyoti and S. G. Singh, *Biosensors and Bioelectronics*, 2019, **124**, 205-215.
15. S. Mahapatra, R. Kumari and P. Chandra, *Trends in Biotechnology*, 2024, **42**, 591-611.
16. H. Shamkhalichenar, C. J. Bueche and J.-W. Choi, *Biosensors*, 2020, **10**, 159.
17. P. Jolly, J. Rainbow, A. Regoutz, P. Estrela and D. Moschou, *Biosensors and Bioelectronics*, 2019, **123**, 244--250.
18. D. Llull, R. Lpez and E. Garca, *Journal of Clinical Microbiology*, 2006, **44**, 1250--1256.
19. S. Campuzano, M. Pedrero, J. L. Garca, E. Garca, P. Garca and J. M. Pingarn, *Analytical and Bioanalytical Chemistry*, 2011, **399**, 2413--2420.
20. N. Woodford, A. Carattoli, E. Karisik, A. Underwood, M. J. Ellington and D. M. Livermore, *Antimicrobial Agents and Chemotherapy*, 2009, **53**, 4472--4482.
21. D. Pletcher, *A first course in electrode processes*, Royal Society of Chemistry, 2009.



22. R. G. Compton and C. E. Banks, *Understanding voltammetry*, World Scientific, 2007. View Article Online  
DOI: 10.1039/D5SD00210A
23. J. Wang, M. C. Leong, E. Z. W. Leong, W. S. Kuan and D. T. Leong, *Analytical Chemistry*, 2017, **89**, 6900--6906.
24. F. P. Ferreira, A. C. Honorato-Castro, J. V. da Silva, S.-C. Orellana, G. C. Oliveira, J. M. Madurro and A. G. Brito-Madurro, *Polymer Engineering & Science*, 2018, **58**, 1308--1314.
25. F. Li, Z. Yu, Y. Xu, H. Ma, G. Zhang, Y. Song, H. Yan and X. He, *Analytica Chimica Acta*, 2015, **886**, 175--181.
26. H. Wang, Z. Ma, J. Qin, Z. Shen, Q. Liu, X. Chen, H. Wang, Z. An, W. Liu and M. Li, *Biosensors and Bioelectronics*, 2019, **126**, 373--380.
27. A. Dobrea, N. Hall, S. Milne, D. K. Corrigan and M. Jimenez, *Scientific Reports*, 2024, **14**, 14154.
28. A. Ainla, M. P. S. Mousavi, M.-N. Tsaloglou, J. Redston, J. G. Bell, M. T. Fernández-Abedul and G. M. Whitesides, *Analytical Chemistry*, 2018, **90**, 6240-6246.
29. K. A. Bautista, E. Madsen, S. D. Riegler and J. C. Linnes, *ACS Electrochemistry*, 2025, **1**, 386-394.
30. F. Gutierrez, M. Mar, J. C. Rodriguez, A. Ayelo, B. Soldn, L. Cebrin, C. Mirete, G. Royo and A. M. Hidalgo, *Clinical Infectious Diseases*, 2003, **36**, 286--292.
31. S. O. Kelley, *ACS Sensors*, 2017, **2**, 193--197.



## Data Availability Statement (DAS)

View Article Online  
DOI: 10.1039/D5SD00210A

Key data that supporting the findings of this study have been included in the manuscript. Additional data that supporting this article have been included as part of the Supplementary Information.

